Int. J. Multiphase Flow Vol. 10, No. 5, pp. 557–569, 1984
Printed in the U.S.A.

0301-9322/84 $3.00 + .00
Pergamon/Elsevier

EXPERIMENTAL AND NUMERICAL INVESTIGATION OF BUBBLE-DRIVEN LAMINAR FLOW IN AN AXISYMMETRIC VESSEL

F. DURST
Lehrstuhl für Strömungsmechanik, Universität Erlangen–Nürnberg, Egerlandstr. 13, D-8520 Erlangen, F.R.G.

and

A. M. K. P. TAYLOR and J. H. WHITELAW
Fluids Section, Department of Mechanical Engineering, Imperial College of Science and Technology, London SW7 2BX, England

(*Received* 22 *July* 1982; *in revised form* 7 *October* 1983)

Abstract—Measurements have been obtained, by laser-Doppler anemometry (LDA), of the axisymmetric, recirculating liquid flow caused by a column of air bubbles (5–6½ mm dia.) rising through caster oil in a cylindrical enclosure (100 mm dia.). The liquid velocities correspond to creeping flow. Axial and radial liquid velocity profiles are reported at eight axial stations and, close to and within the bubble column, as a function of time. The maximum liquid velocity found outside the bubble column is about 0.5 of that of the bubbles and a very rapid radical decay from this value is noted. The temporal variation of the velocity field, due to the passage of the air bubbles, is undetectable at radial locations greater than about 1½ bubble radii from the centreline.

The variation of bubble velocity with axial distance was also measured by LDA for liquid height to enclosure diameter ratios of 0.98 and 2.78. The maximum bubble velocities were about 0.1–0.2 higher than the Stokes law terminal velocity. The increase is due to the convection of the bubble column by the liquid flow. The maximum bubble velocity is established within approximately three bubble diameters of the air inlet.

The motion of the liquid has been calculated by the numerical solution of the steady form of the equations of motion, with the inner boundary of the area of integration lying 1.3 bubble radii from the centerline. The boundary conditions at this surface are assumed to be steady and are taken from measurements of the time-averaged velocity components. The assumption of steady flow at this boundary is supported by experimental observation and results in calculations which are generally in close agreement with the measurements. Discrepancies are confined to the immediate vicinity of the bubble column near to the top and bottom of the enclosure. These are ascribed to a combination of small asymmetries in the experiment and inadequate numerical resolution in these regions.

1. INTRODUCTION

Bubbling of gas into a liquid occurs in natural waters and finds numerous industrial applications: e.g. in a gas absorption and oxidation equipment, in bioreactors and fermentation columns, in liquid metal containers during steel making and in water reservoirs during destratification. In all of these applications, advancements of today's technology can only be achieved through more detailed information on the local velocity and size of rising bubbles and on the entire induced flow field of the fluid. Numerous investigations of bubble flows have been carried out and attempts made to employ the resultant information to describe inter-phase heat, mass and momentum transfer and to develop calculation methods for multi-phase flows. Bubble flows represent only *one* class of multi-phase flows, but an important one for many industrial applications. In spite of this importance, the availability of detailed local information on bubble size and bubble velocity, as well as local fluid velocity, is scarce due to the lack of suitable measuring techniques.

Under some flow conditions it is possible to make use of the laser–Doppler anemometer and its development for use in two-phase flows has been pursued in recent years by a number of workers (e.g. Lee & Srinivansan 1982; Durst *et al.* 1982), the present work is based on the work of Durst & Zaré (1975) who showed that the velocity, size and concentration of large particles (e.g. a gas bubble in a liquid flow) could be measured using an extended conventional laser–Doppler system.

This paper describes the use of the laser–Doppler aneomometer in a simple two-phase flow and presents velocities in an axisymmetric, recirculating liquid flow caused by a steady column of air bubbles rising through castor oil in a cylindrical enclosure. The results contribute to the existing knowledge of simple bubble motions in liquids. For example, unconfined, turbulent bubble plumes have been measured by Chesters *et al.*(1980) using a laser–Doppler anemometer for the continuous phase. When the bubble column is confined, the liquid phase is usually arranged to recirculate and this phenomenon can affect the gas hold-up. A few velocity profiles in the confined case, using a modified Pitot probe, have been reported by Hills (1974) and Pavlov (1965) and Pozin *et al.* (1969) (both cited by Hills 1974). Rietema & Ottengraf (1970) used particle tracking to provide similar information in laminar flow.

The calculation of bubble-driven liquid flow has been considered by a number of authors (e.g. Freedman & Davidson 1969; Rietema & Ottengraf 1970; Ueyama & Miyauchi 1979), although simplifying assumptions were required to allow analysis to proceed. For example, the latter two references consider the flow occurring far from the top and bottom of the liquid column, so that radial pressure gradients could be neglected. The present paper reports calculations of the liquid flow by numerical integration of the steady, two-dimensional forms of the continuity and momentum equations. Boundary conditions were specified at the test section walls and, from the experiments, at fixed boundaries inside the liquid flow.

Details of the experimental equipment and the laser–Doppler anemometer are given in the following section. Section 3 presents the experimental results, describes the numerical calculation procedure and compares the predictions with the measurements. Concluding remarks are provided in section 4.

2. FLOW CONFIGURATION AND EXPERIMENTAL METHOD

2.1 *Flow configuration*

The flow was established in a glass cylinder of 100 mm i.d. with bubbles forming at a 0.5 mm dia. nozzle located on the axis of the cylinder, as shown in figure 1. The tube contained castor oil, of which the kinematic viscosity (0.699×10^{-3} m^{3}s^{-1}, measured at 25°C) was sufficiently large to guarantee laminar liquid flow and also nonspiral motion of the rising air bubbles. Air was passed through an accurate, well controllable pressure regulator and the resulting bubbles left the nozzle at a steady rate of one every 0.55 s. with a diameter of about 5–6½ mm. This was the minimum period of formation for which a regular "street" of spherical bubbles, rising through the liquid column, could be maintained without coalescence. The period of bubble formation was continuously monitored and kept constant throughout the experiment. Two liquid heights were investigated (z_T = 0.098 and 0.278 m) corresponding to ratio of the liquid height-to-tube diameter of 0.98 and 2.78.

The cylinder was enclosed in a plane-sided trough, as shown in figure 1, with the space between the trough and the cylinder occupied by castor oil. The refractive index of this oil (n_D = 1.477) is very close to that of glass, so that there was no refraction of the laser beams and consequently no corrections had to be applied to the measuring location when radial profiles were taken. The location of the measuring volume was taken from the dials of a three-dimensional traverse table on which the entire test section was mounted. All readings were taken relative to the location of the nozzle exit, so that z = 0 and r = 0 were fixed at the nozzle centre and the upper part of the nozzle mouth.

2.2 *Laser–Doppler anemometer and signal processing*

The velocities of both the phases were measured with the laser–Doppler anemometer depicted in figure 2. As far as the measurements in the liquid phase are concerned, the principles of the anemometer can be found in Durst *et al.* (1981) and are not repeated here.

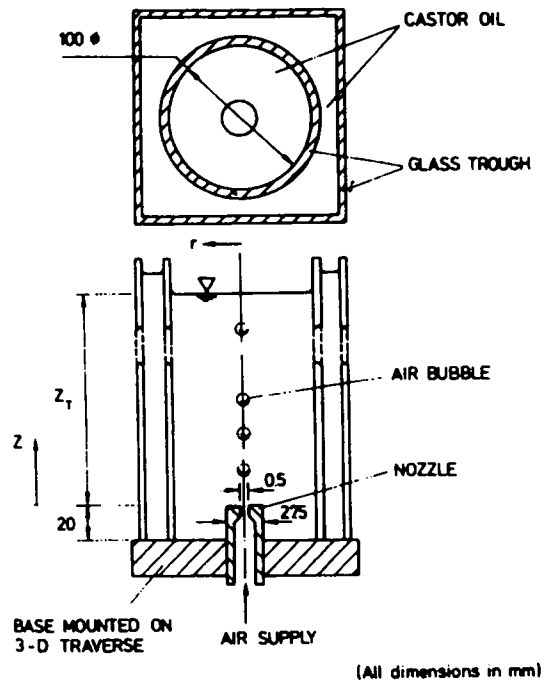

Figure 1. Scheme of flow configuration.

The presence of recirculation in this phase requires the use of light frequency shifting to distinguish between positive and negative velocities and this was derived from two acousto-optic modulators ("Bragg" cells), each arranged to provide frequency shifts in the 38–40 MHz range, with an accuracy of better than one part in 10^6: the exact value of the shift was monitored by a frequency counter. The principal characteristics of the anemometer are given in table 1.

The liquid was seeded with titanium dixoide particles (nominal diameter less than 2 μm to provide scattering centres in sufficient concentration to result in a near continuous Doppler signal. This signal was detected by a photomultiplier tube, conditioned as shown in figure 2, and then used to drive the voltage-controlled oscillator (VCO) of a tracker (BBC–Goerz type LSE/01). The output of the VCO (continuous and of constant amplitude)

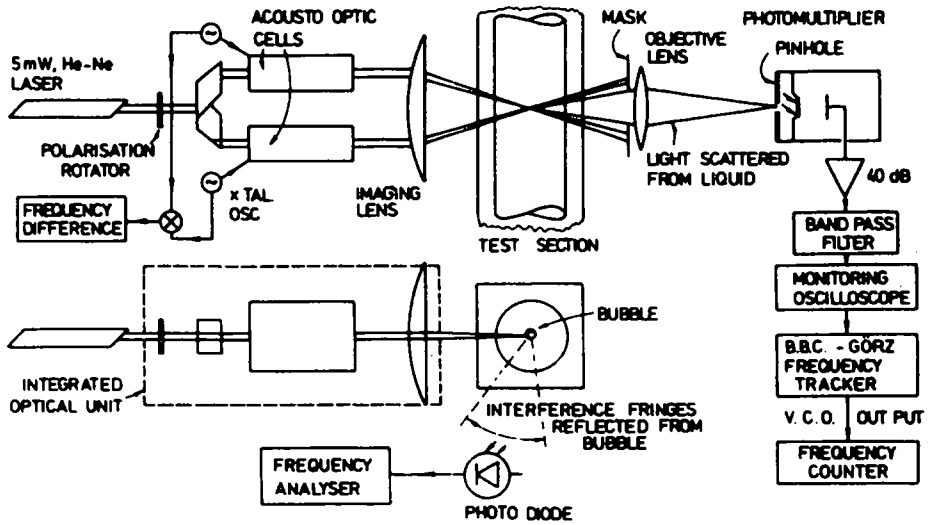

Figure 2. Laser–Doppler anemometer and associated signal processing for liquid and gas phase velocities.

Table 1. Characteristics of laser–Doppler anemometer

Half angle of intersection (degrees, in air)	5.76
Fringe separation in measuring volume (μm)	3.15
Measuring volume diameter calculated at $1/e^2$ intensity (mm)	0.15
Measuring volume length calculated at $1/e^2$ intensity (mm)	1.5
Transfer constant (MHz/ms^{-1})	0.317
Nominal frequency shift (KHz)	25 and 50

was processed by a frequency counter to give the Doppler frequency. The "self-adjust" facility of this tracker was used to make sure that the centre of the IF filter stage did not drift over long measurement times.

The measurement of the axial (W) and radial (V) components of velocity was achieved by rotation of the integrated optical unit about its axis. The effects of velocity gradient broadening was rendered negligible by aligning the minor axis of the measuring volume with the direction of the largest velocity gradient.

The extension of the anemometer to the measurement of bubble velocity, which involves no new physical principle, has been described by, e.g. Durst & Zaré (1975). Briefly, when the two laser beams are incident on the bubble surface, light is reflected (and refracted) so that an interference pattern is formed in space. The fringes of this pattern move such that the frequency with which these pass a fixed point in space, for example the pinhole of a photodetector, is linearly related to the bubble velocity. The signal from the dispersed phase is distinguished from that of the liquid by a separate detection system (a photodiode) located approximately at right angles to the axis of the anemometer, as shown in figure 2. The photodiode was not sensitive to the light scattered by the titanium dioxide particles because of its low intensity and only recorded the passage of the bright interference pattern produced by the bubbles. The frequency of the signal was processed by spectral analysis using a Hewlett–Packard spectrum analyser model 8552A/8553B.

3. RESULTS AND DISCUSSION

3.1 *Flow visualisation*

The general flow pattern which is induced by the rising bubble street (in a liquid column of 27.8 cm) is shown in figure 3(a). The visualisation was made by introducing microcopic air bubbles (less than 0.3 mm dia.) and illuminating the cylinder across a diametral plane. The exposure was set at the time taken for a bubble in the column to rise through the liquid: the bright vertical column visible in the photograph is the long-term exposure of the bubble street. The flow is dominated by a single recirculation cell with smaller, subsidiary "convection cells" (Tritton 1977) sometimes visible along the length of the locus of zero vertical velocity. Additional cells may also be induced by measuring probes as demonstrated in figure 3(b) which shows the extent of the distrubance which occurs at Reynolds numbers that correspond to creeping flow.

3.2 *Velocity profiles of gas and liquid phases*

The axial variation of the bubble velocity is depicted in figure 4 for the two liquid heights: the maximum velocity attained is greater for the larger liquid height ($W_{B,\max}$ – 3.34 vs 3.09 cm s^{-1}). The bubbles move at a Reynolds number ($a\,W_{\nu,\max}/\nu$) of approx. 0.14, for which Stokes' law is appropriate. The terminal velocity is about 2.8 cm s^{-1} for a single unconfined bubble of 6 mm dia. rising in a stagnant liquid assuming that the interface is rigid, the bubbles are assumed to behave as rigid spheres because it is likely (see section 3.3 below)

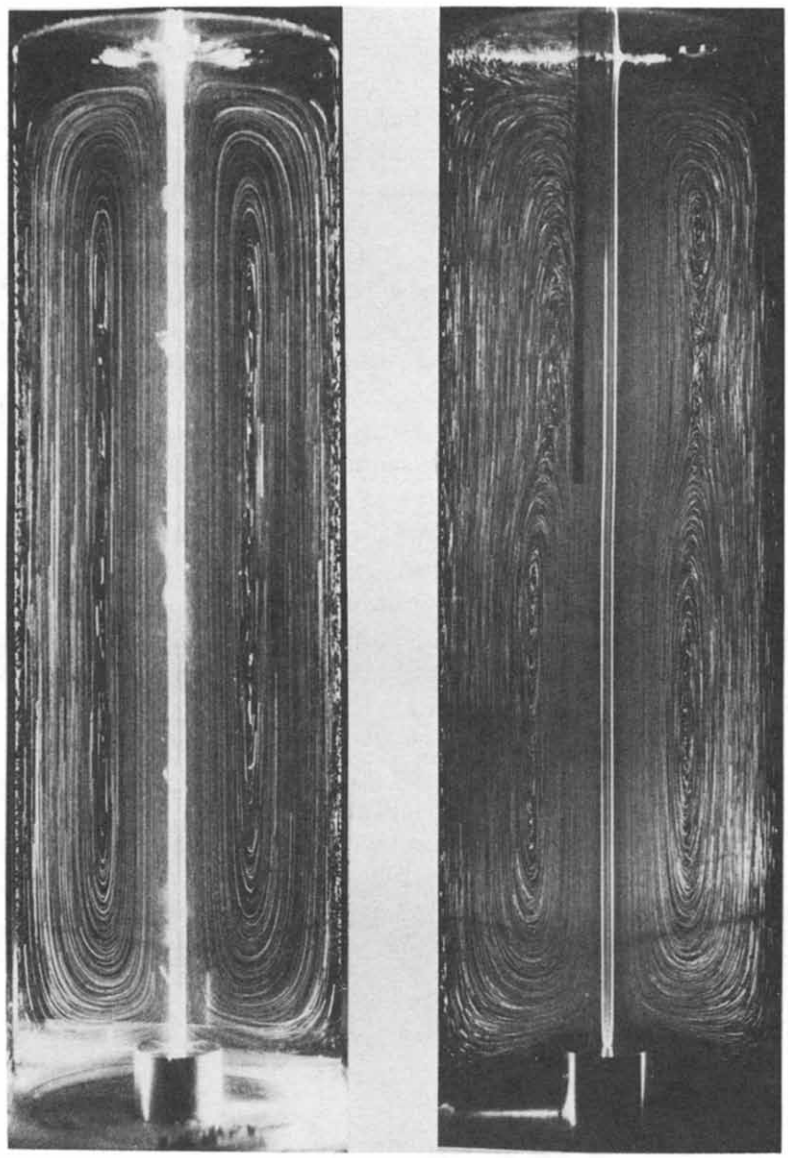

Figure 3. Streaklines, visualized by air bubbles, of flow in cylinder: liquid height 0.278 m (a) normal flow; (b) disturbance produced by a probe inserted through free surface.

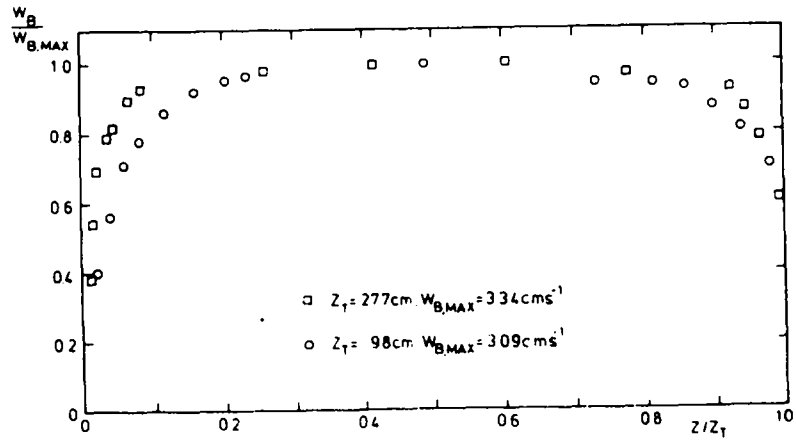

Figure 4. Axial (centre-line) development of bubble velocity for two liquid heights.

that the titanium dioxide particles caused the air–liquid interface to act as a rigid surface as mentioned, for example, by Batchelor (1967). The experiment shows that the bubble street rises at velocities about 0.1–0.2 cm s^{-1} higher than this value for the smaller and larger liquid heights respectively; this is due to the liquid motion in the cylinder convecting the bubbles. However, the appropriate value of the terminal velocity is uncertain due to the tolerance on the diameter of the bubbles. It is noted that the distances over which the bubbles accelerate (near the nozzle) and decelerate (near the free surface) are influenced by local conditions and hence do *not* scale with the total height of liquid, z_T. Thus about 0.9 of the maximum bubble velocity is achieved in less than three bubble diameters away from the nozzle and free liquid surface for both values of z_T.

Measurements of the liquid velocity were obtained across the diameter of the tube and confirmed that the only region of asymmetry was confined to the vicinity of the bubble column near the free surface. Detailed liquid-velocity profiles were measured for both liquid column heights but since these do not reveal substantial differences, only the profiles for the lower (z_T = 9.8 cm) liquid column are presented here. The radial profiles of axial velocity, figure 5, show that the maximum liquid velocity which was measured as only about one half that of a bubble, with a very rapid radial decay of velocity away from the rising bubbles. The recirculating flow is confirmed by the measurements and, as expected, the negative velocities are about one tenth of the magnitude of the positive ones. (The difference in the magnitudes is expected, in axisymmetric geometries, because the negative velocities can flow over much larger areas than can the positive velocities.) The influence of the nozzle on the profile nearest to it can be detected. The radial velocity profiles, figure 6, show that particularly large values occur near the free surface as the axial flow, entrained by the bubble column, approaches the free surface and is deflected radially.

The bubble street gives rise to a liquid velocity field which is, at least near the axis of symmetry, strongly time-dependent. This is shown on figures 7 (a)–(d) which are the

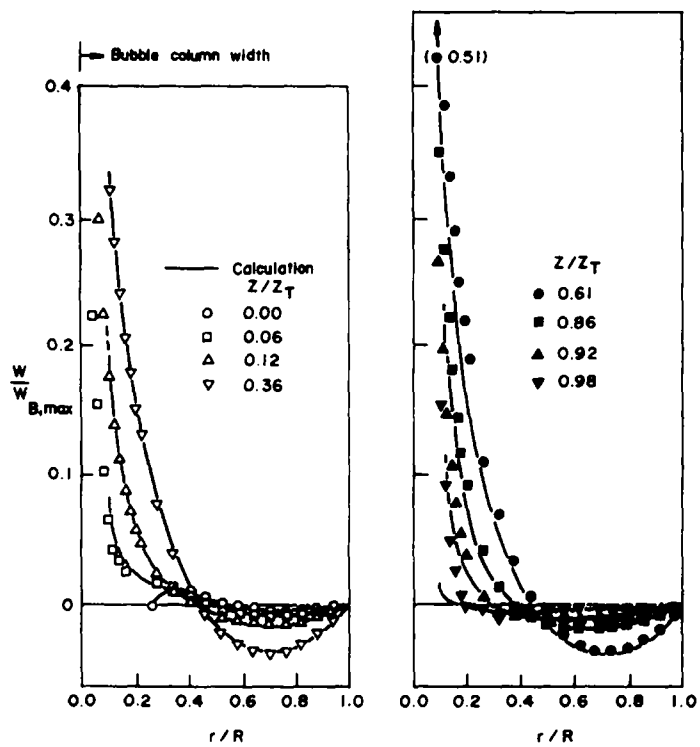

Figure 5. Profiles of axial velocity of liquid phase successive axial stations. Total liquid height z_T, is 0.098 m. Curves represent results of calculations.

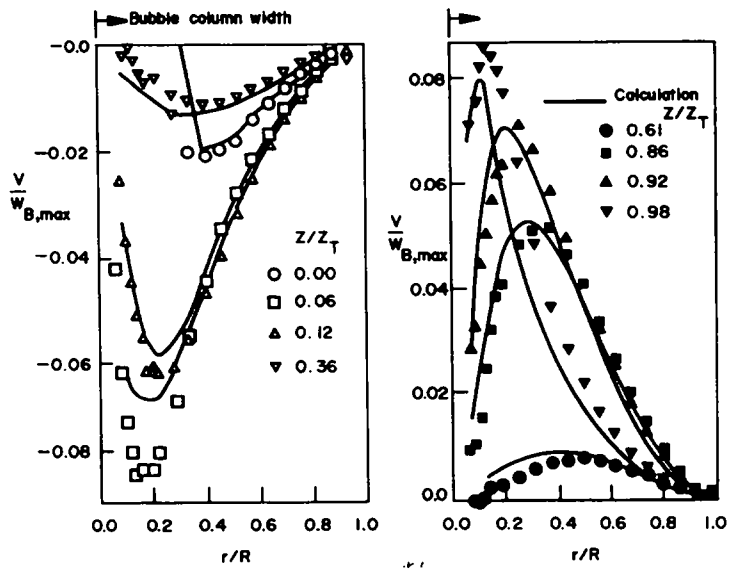

Figure 6. Profiles of radial velocity of liquid phase at successive axial stations. Total liquid height, z_T is 0.098 m. Curves represent results of calculations.

Doppler frequency-analogue outputs of the tracker recorded at four radial positions. When the measuring volume is placed in the bubble column, figure 7(a), the occurrence of a bubble displaces the measuring volume and light is no longer scattered in the direction of the photomultiplier. As a result there is no signal for the tracker to demodulate and the frequency-analogue output is "frozen" to the last velocity value, until the bubble passes and a liquid-phase Doppler signal is again available. It is noted that the exception to this remark is when the measurement takes place on the center-line, in which case interference of light, refracted in the forward direction, can be detected by the photomultiplier, as discussed by Martin *et al.* (1981). On the center-line, the refracted interference pattern motion is demodulated and gives rise to the variation of the tracker output, noted in the centre of figure 7(b).† At locations closest to the center-line the liquid velocity, between successive bubbles, is seen to vary from a maximum corresponding to the bubble velocity to only one fifth of that value. At radial locations larger than the radius of the bubble column, these variations are rapidly damped and are virtually undetectable at $r = 0.08R$, figure 7(d), so that although the passage of bubbles is not a steady phenomenon, the net effect on the flow is, even at distances of about one bubble diameter away from the bubble column. This observation is important for the specification of boundary conditions in the calculations presented in sub-section 3.3.

The large viscosity of the liquid is responsible for the strong damping of the velocity fluctuations induced by each bubble, quantitative assessment of the damping can be made from the analytical solution (Batchelor 1967) of the flow due to a boundary which oscillates in its own plane. The velocity fluctuations propagate away from such a boundary, into the fluid, as damped transverse waves such that the amplitude of the velocity fluctuations falls off with distance (y) from the disturbance as:

$$\exp\{-(w/2\nu)^{1/2}y\} \qquad [1]$$

where w is the angular frequency of the oscillation. The magnitude of this damping term is such that velocity fluctuations penetrate for less than one wave-length into the fluid, which

†An independent estimate of the bubble velocity can be made from the time interval during which there is no signal and the diameter of the bubble. The interval in figure 7(b) is consistent with the velocity measured from the Doppler frequency, given a bubble diameter of 5 mn.

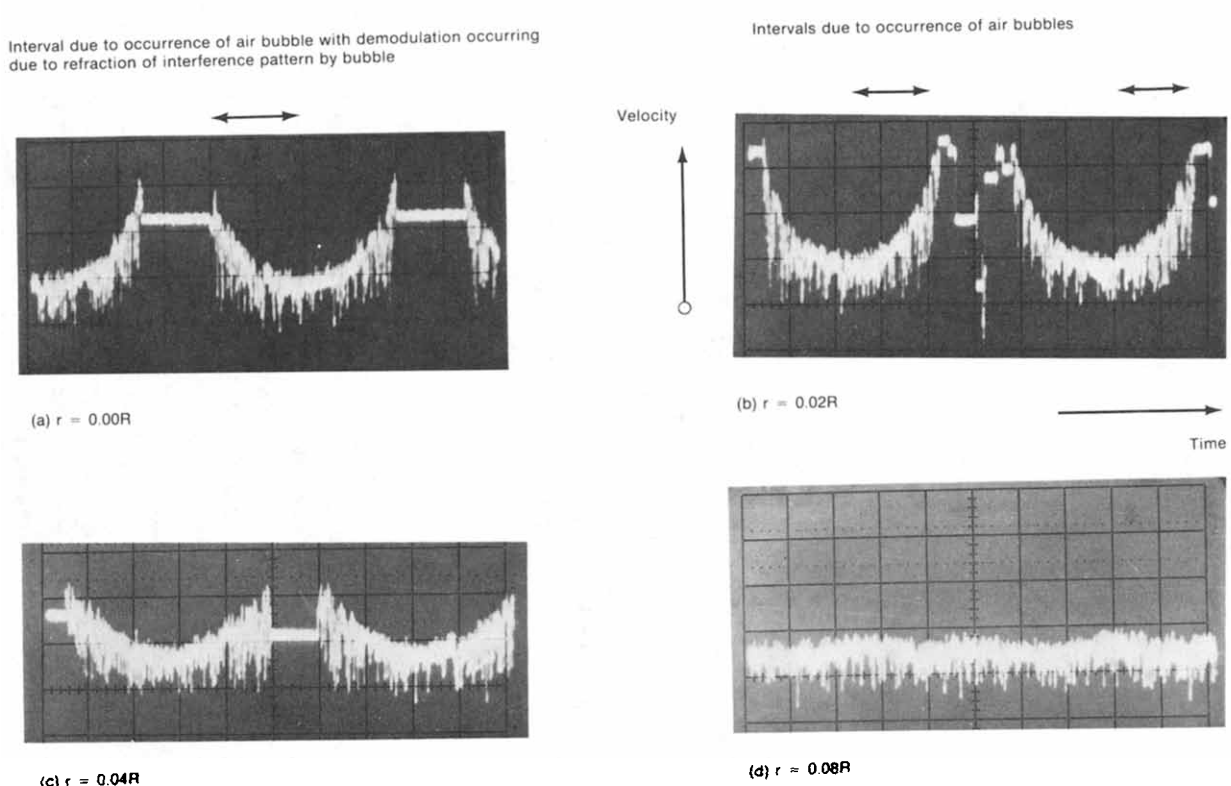

Figure 7. Time-resolved liquid axial velocity at $z = 0.49\ z_T$, at four radial positions, $z_T = 0.98$ m. (Vertical division equivalent to 0.23 $W_{z,max}$, origin at horizontal graticule. Horizontal division equals 0.1 s.)

(at least for plane flow) is of the order of $(\nu/w)^{1/2}$. In the present case, this is a distance of about 7 mm.

Figure 8 shows the time-dependent liquid velocity at a location close to the nozzle exit. The occurrence of the velocity excursion between bubbles is interpreted as the motion caused by the abrupt growth of a new bubble at the nozzle. It is noted that the noise associated with the frequency-analogue voltage of the tracker is not relevant to the velocity profiles of figures 5 and 6 which were obtained by frequency counting.

3.3 *Calculation of the liquid flow*

This sub-section describes the way in which the partial differential equations of motion were integrated and presents the comparison with experiment. Let the pressure be designated by p. If the liquid flow is assumed to have constant properties, be incompressible, steady and axisymmetric with no azimuthal component of velocity and free of body forces, then the following equations are appropriate:

Conservation of mass:

$$\frac{\partial W}{\partial z} + \frac{\partial V}{\partial r} + \frac{V}{r} = 0. \qquad [2]$$

Conservation of axial momentum:

$$\frac{\partial}{\partial z}(W^2) + \frac{1}{r}\frac{\partial}{\partial r}(rVW) = -\frac{1}{\rho}\frac{\partial p}{\partial z} + 2\nu\frac{\partial^2 w}{\partial z^2} + \frac{\nu}{r}\frac{\partial}{\partial r}\left[r\left(\frac{\partial V}{\partial z} + \frac{\partial W}{\partial r}\right)\right]. \qquad [3]$$

Conservation of radial momentum:

$$\frac{\partial}{\partial z}(VW) + \frac{1}{r}\frac{\partial}{\partial r}(rV^2) = -\frac{1}{\rho}\frac{\partial p}{\partial r} + \nu\frac{\partial}{\partial z}\left(\frac{\partial V}{\partial z} + \frac{\partial W}{\partial r}\right) + 2\nu\frac{\partial^2 V}{\partial r^2} + \frac{2\nu}{r}\left(\frac{\partial V}{\partial r} - \frac{V}{r}\right). \qquad [4]$$

Boundary conditions for W and V are required along the closed curve describing the boundary of the area of integration. These were applied as follows:

(a) solid surface—zero normal and tangential velocities:

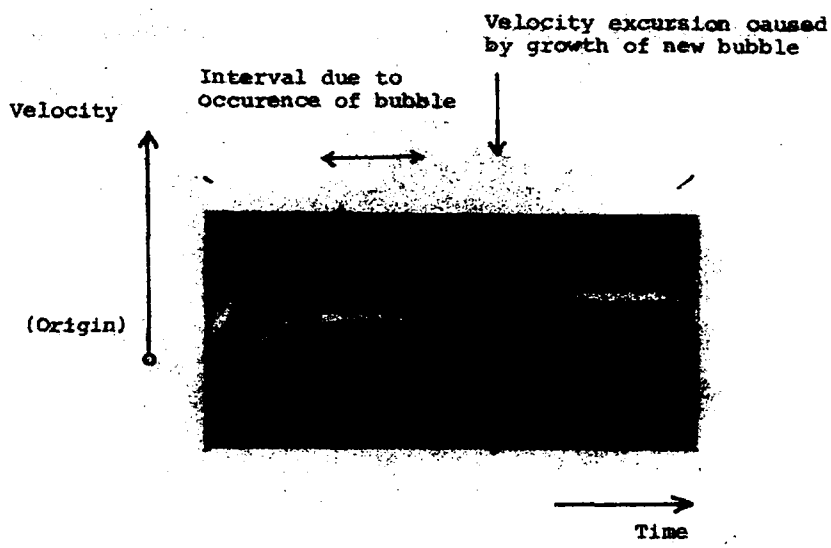

Figure 8. Time-resolved liquid axial velocity at $z = 0.06\, z_T$, $r = 0.0R$. Axes as for figure 7.

(b) line at $r = 0.08R$—the time-average of the measured values of W and V at $r = 0.08R$. It is noted that, for reasons of mass conservation, the experimental profile of radial velocity must satisfy $\int_0^{z_T} V(z)\,dz = 0$;

(c) free surface at $z = z_r$—zero velocity both along and normal to the surface. The alternative boundary condition of zero surface shear stress was also used, but resulted in slightly poorer agreement with the experiment. This is discussed in the following paragraph. These three equations were solved with a form of the calculation method reported by Gosman & Pun (1973). The following paragraph briefly outlines the solution procedure.

The numerical procedure solves finite-difference equations for the primitive (W, V, p) variables. The area of integration (figure 9) is overlayed with a cartesian, non-uniform grid (29 grid lines in the axial and 22 in the radial direction) with the velocity variables being staggered with respect to pressure, which is located at the grid nodes. It is noted that the inner boundary lies outside the rising bubble column, at about 1.3 bubble radii ($0.08R$). Using the "hybrid-differencing" scheme (Spalding 1972) a set of implicit, linearised algebraic equations was solved interatively, see Patankar & Spalding (1972), using a line-by-line application of the tri-diagonal matrix algorithm, starting from guessed values of W, V and p. The equivalent of the continuity equation, called the pressure-correction equation, adjusts the guessed pressure and velocity fields and moves the solution field closer to simultaneous satisfaction of the equations of motion.

The results of the calculation, shown in figures 5 and 6, are in close agreement with experiment the greatest discrepancies are to be found near the bubble column at the top and bottom of the enclosure. One reason for the disagreement near the top, that is near the free surface, is the slight asymmetry in the flow (at $z = 0.98\ z_T$), so that the values of $W(r = 0.08R)$ and $W(r = 0.08R)$ are different. Since the average of these two values was used as a boundary condition, there is a difference between measurement and calculation even at the boundary (apparent in figure 5). Another reason is that the finite difference mesh which was used may not have been sufficiently fine to resolve adequately the rapid axial, as well as radial, variations in the flow field in these regions. "Numerical diffusion" due to the use of upwind differencing for the convective terms, which is often an important source of error in calculations of high Reynolds number recirculating flows e.g. McGuirk *et al.* (1982), is not a problem here. This is because central differentiating is used everywhere (because the computational cell Péclet number is $\simeq 10^{-3}$) and, in any case, convection is negligibly small compared to the pressure gradient and diffusion terms.

The boundary conditions which were used along the bubble column and at the free surface merit some discussion. The measured axial profiles of W and V at $r = 0.08R$ refer to

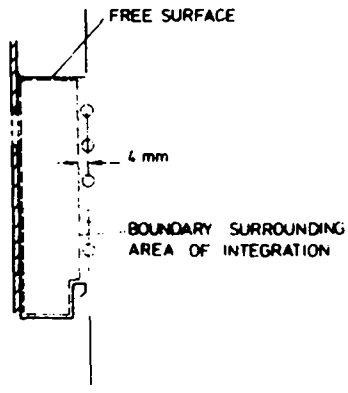

Figure 9. Diagram defining area of integration (n.b. boundary coincides with solid and free surfaces).

time-mean values. Experiment shows that the velocity fluctuations due to the passage of bubbles are small by this position (see figure 7d) so that the assumption of steady flow is a good approximation, particularly since these are regions of large velocity gradient where the viscous stress is large in comparison with the "Reynolds" stress. That the assumption of zero surface velocity at the free surface gave better agreement with experiment than was the case when zero surface shear was applied may be supported by the observation (e.g. Batchelor 1967) that impurities in a liquid can cause an air-liquid interface to act as a partially rigid surface. In this case the addition of seeding particles (for the anemometer) and the absorption of impurities from the laboratory atmosphere has probably had this effect, although the behaviour of the free surface was not studied in this work.

4. CONCLUDING REMARKS

1. The results of the preceding sections have shown that laser–Doppler anemometry can be used, as suggested by Durst & Zaré (1975), to measure the rising velocity of bubbles and the velocity field of the liquid.

2. (a) The maximum bubble velocities are 3.1 and 3.3 cm/s for the smaller (z_T = 9.8 cm) and larger (z_T = 27.8 cm) liquid heights respectively. These values are between 0.1 and 0.2 cm s^{-1} higher than the Stokes' terminal velocity and show the magnitude of the influence of the liquid convection in increasing the bubbles' rising velocity. Ninety per cent of the terminal velocity is observed within less than about three bubble diameters away from the nozzle exit and free liquid surface.

(b) The unsteady component of the liquid velocity field decays rapidly with radial distance away from the bubble column and is virtually undetectable at about 1½ bubble radii from the center-line. The rapid spatial decay of the velocity fluctuations is due to viscous damping.

(c) The profiles of axial velocity show that the liquid in the immediate vicinity of the bubbles undergoes large shear, and the maximum liquid velocity which was measured was only one half of the maximum bubble velocity.

3. The liquid motion has been calculated with the assumption that the velocity is steady at the inner boundary which lies at 1.3 bubble radii from the centerline. Discrepancies are confined to the vicinity of the bubble column near to the top and bottom of the enclosure. These are ascribed to a combination of small asymmetries in the experiment and to inadequate numerical resolution in these regions, the assumption of steady flow at the inner boundary is supported by 2(b) above.

4. It is to be expected that the present work can be extended to higher speeds, to polydisperse bubbles and to the further investigation of the bubble-wake region. The ranges of void fractions and of optical path length for which such measurements are possible will be limited by the signal attenuation caused by bubbles in each laser beam: these effects remain to be quantified.

Acknowledgements—The research described in this paper is the outcome of a cooperative program between the Sonderforschungsbereich 80 of the Universität Karlsruhe and the Fluids Section of the Department of Mechanical Engineering at Imperial College. We gratefully acknowledge the Deutsche Akademische Austauschdienst (DAAD) for the financial support of A. Taylor during his stay at the University of Karlsruhe.

NOTATION

Roman characters

- a bubble radius (≃0.003 m)
- p pressure

R radius of cylindrical enclosure
r radius co-ordinate direction (origin: figure 1)
t time
V time-mean radial velocity component
W time-mean axial velocity component
z axial co-ordinate direction (origin: figure 1)

Greek character

ν kinematic viscosity of castor oil

Subscripts

B bubble
B, max maximum bubble axial velocity
T total liquid height

REFERENCES

BATCHELOR, G. K. 1967 *An Introduction to Fluid Dynamics.* Cambridge University Press.

CHESTERS, A. K., VAN DOORN, M. & GOOSENS, L. H. J. 1980 A general model for unconfined bubble plumes from extended sources. *Int. J. Multiphase Flow* **6**, 499–521.

DURST, F., MELLING, A. & WHITELAW, J.H. 1981 *Principles and Practice of Laser–Doppler Anemometry,* 2nd Edn. Academic Press, London.

DURST, F. & ZARÉ, M. 1975 Laser–Doppler measurements in two-phase flows. *Proc. of the LDA-Symp.* (Edited by P. Buchhave *et al.*), pp. 403–429, Copenhagen 1975, P.O. Box 70, DK–2740 Skovlunde, Denmark.

FREEDMAN, W. & DAVIDSON, J. F. 1969 Hold-up and liquid circulation in bubble columns. *Trans. Instn. Chem. Engrs.* **47**, T251–T262.

GOSMAN, A. D. & PUN, W. M. 1973 Lecture notes for a course entitled "Calculation of recirculating flows". *Heat Transfer Section Report HTS/74/2.* Dept. of Mechn. Engng, Imperial College, London.

HILLS, J. H. 1974 Radial non-uniformity of velocity and voidage in a bubble column. *Trans. Inst. Chem. Engrs.* **52**, 1–9.

LEE, S. L. & SRINIVASAN, J. 1982 An LDA technique for *in situ* simultaneous velocity and size measurement of large spherical particles in a two-phase suspension flow. *Int. J. Multiphase Flow* **8**, 47–57.

MARTIN, W. W., ABDELMESSIH, A. H., LISKA, J. J. & DURST, F. 1981 Characteristics of laser–Doppler signals from bubbles. *Int. J. Multiphase Flow* 7, 439–460.

MCGUIRK, J. J., TAYLOR, A. M. K. P. & WHITELAW, J. H. 1982 The assessment of numerical diffusion in upwind difference calculations of turbulent recirculating flow. In *Turbulent Shear Flows* 3 (Edited by L. J. S. Bradbury *et al.*), pp. 206–224. Springer-Verlag, Berlin.

PATANKAR, S. V. & SPALDING, D. B. 1972 A calculation procedure for heat mass and momentum transfer in three dimensional parabolic flows. *Int. J. Heat Mass Trans.* **15**, 1787–1806.

PAVLOV, V. P. 1965 *Khim. Prom.* **9**, 698.

POZIN, L. S., AEROV, M. E. & BYSTROVA, T. A. 1969 *Theoretical Foundations of Chem. Engng.* **3**, 714.

RIETEMA, K. & OTTENGRAF, S. P. P. 1970 Laminar liquid circulation and bubble street formation in a gas–liquid system. *Trans. Inst. Chem. Engrs* **48**, T54–T62.

SPALDING, D. B. 1972 A novel finite difference formulation for differential expressions involving both first and second derivatives. *Int. J. Numer. Meth. Engng.* **4**, 551–559.

TRITTON, D. 1977 *Physical Fluid Dynamics*. Van Nostrand Reinhold, New York.

UEYAMA, K. & MIYAUCHI, T. 1979 Properties of recirculating turbulent two-phase flow in gas bubble columns. *AIChE J.* **25**(2), 258–266.